Aligned Magnetic Field-Enhanced MHD Mixed Convection and Heat Transfer on a Moving Inclined Porous Surface

W.Sridhar[1*] ,D..Srinivasa Rao[2],g.Dharmaiah[3],V.Sujatha[4]

[1]Department of Mathematics, Koneru Lakshmaiah Education Foundation, Vaddeswaram, Guntur, A.P., India

[2]Department of Mathematics, Aditya College of Engineering and Technology,Surampalem,E.G.Dist, A.P., India

[3]Department of Mathematics, Narsaraopet Engineering College, Narsaraopet, Guntur, A.P., India

[4] Department of Mathematics, YSR Engineering College Of Yogi Vemana universityProddutur,A.P.,India

*Corresponding Author:sridharwuriti@gmail.com

Abstract: The primary objective of this study is to investigate the combined effects of magnetohydrodynamic (MHD) mixed convection flow along with heat transfer on an inclined permeable sheet in motion, subjected to an aligned magnetic field. To attain this goal, precise solutions for the partial differential equations (PDEs) are derived using perturbation techniques. The research explores the impact of several factors, including radiation thermo, chemical reaction, Hall current and the aligned magnetic field. Notably, it is noted that higher values of the Schmidt number (Sc) and the parameter γ lead to a reduction in fluid concentration. Conversely, elevated values of parameters ϕ, Prandtl number (Pr), and the mixed convection parameter (F) result in a decrease in temperature. The velocity of the fluid is found to increase with higher values of the Grashof numbers (Gr), Görtler numbers (Gc), thermal buoyancy parameter (α), mixed convection parameter (F), and the permeability parameter (K). On the contrary, the velocity decreases when parameters of non-dimentional such as the Hartmann number (M), Sc, Pr, ξ, power-law index (m), and ϕ are increased. Further analysis reveals that the Sherwood number experiences a decline with increasing Sc and γ values. Conversely, the Nusselt number rises as the parameters F, ϕ, and Pr increase. Additionally, the study shows that an increase in the permeability parameter (K), Gr, and Gc results in a higher skin-friction coefficient, whereas an increase in parameters M, α, F, Sc, m, and ξ leads to a decrease in the skin-friction coefficient. To validate the findings, graphs are generated and compared with the calculated results. In summary, the study sheds light on the interplay between mixed convection, heat transfer, MHD effects, and aligned magnetic fields in a porous medium, providing valuable insights into the intricate fluid dynamics and thermal behavior.

Keywords: mixed convection, heat transfer, magnetohydrodynamics (MHD), aligned magnetic field, porous media

1. INTRODUCTION

The convection of heat and mass across inclined porous surfaces finds numerous applications across various scientific disciplines and technological domains, including chemical industries, nuclear reactor cooling, MHD power generation, geothermal energy extraction, and petroleum engineering. Contemporary research has placed a significant focus on investigating convective heat and mass transfer phenomena involving different physical properties, especially concerning horizontal and vertical flat plates. This research delves into the intricate interaction between Hall current and the flow of magnetic fluid aligned within porous media. The study highlights the ongoing relevance of thermal radiation's effect on unsteady forced convection under the influence of an aligned magnetic field. Both magnetic and aligned electric fields emerge as pivotal factors in fluid dynamics, disrupting the frozen field condition and thus facilitating the dissociation of plasma elements. This disruption causes the breakdown of equi-potential mapping, effective particle acceleration, and quick magnetic energy release.These aligned electric fields are produced by a variety of processes, including turbulence of the waves, solitary objects, magnetic trap, electrical diffuse double layers, and dynamic trapping. The existence of electric fields that are in line with the magnetic field is of utmost importance in the setting of collision-free space plasma.To maintain brevity, the term "parallel" is used interchangeably with "aligned with the magnetic field."

The continuous presence of a non-vanishing electric field aligned with the magnetic field requires a constant balance of momentum imparted to charged particles. This equilibrium can take on various forms of electric fields aligned with the magnetic field, each characterized by distinct features, such as forces originating from the Alternating current electric fields, forces influenced by the DC magnetic field, and the inertial forces.

Recent scientific investigations have extensively explored these concepts. Chamkha et al. [1] conducted numerical analyses concerning chemical reactions and the impacts of thermal radiation. Meanwhile, Rees and Pop [2] undertook simulations to examine the effects of variable permeability. Ingham et al. [3] delved into the study of viscous dissipation within a porous medium confined between parallel plates. Umavathi et al. [4] focused on the effects of unsteady oscillatory flows within a horizontally-oriented composite porous medium channel. Chamkha et

al. [5] investigated how radiation affects the flows of non-Newtonian fluids with both aiding and opposing external flows.

Despite these efforts, relatively less attention has been directed toward boundary layer flows adjacent to inclined plates. Noteworthy is the work of Hossain [6], who explored the impact of Ohmic heating on magnetohydrodynamic (MHD) free convection heat transfer within a Newtonian fluid. Furthermore, studies by Hossain and Gorla [7], Beg et al. [8], Chen [9], Reddy et al. [10], Sibanda and Makinde [11], Wang et al. [12], Yia [13], Choudhury and Das [14], Raju et al. [15], and other researchers have contributed valuable insights to this field.

The main goal of this article is to comprehensively examine how the interaction of mixed convection, radiation thermo, chemical reactions, Hall current, and an aligned magnetic field influences the fluid flow of a viscous, dense, and electrically conductive liquid over a porous flat plate that is both inclined and in motion. Employing perturbation techniques, the complex system of coupled partial differential equations is addressed, ultimately leading to the derivation of analytical solutions.

2. MATHEMATICAL FORMULATION

Consider a scenario involving a laminar boundary layer flow driven by free convection. In this situation, a viscous, incompressible, electrically conducting, chemically reactive fluid is in motion. This fluid is also capable of absorbing and radiating heat. It interacts with a semi-infinite permeable plate with angle of inclination α vertically. This plate is positioned within a uniform porous medium. The entire system experiences the combined effects of thermal buoyancy and concentration buoyancy, furthermore Joule's dissipation. The wall's temperature is maintained at Tw, which is higher than the surrounding ambient temperature T∞. Additionally, the wall's concentration, denoted as C_w, is more than the concentration ambient C∞. It's important to note that a homogeneous first-order chemical reaction takes place between the diffusing species and the fluid, with a rate constant characterizing this reaction. Considering these circumstances, the governing equations for the fluid within a Cartesian system of reference are provided here.

$$\frac{\partial v}{\partial y} = 0 \quad \Rightarrow \quad v^* = -V_0 \tag{1}$$

$$\rho v^* \frac{\partial u^*}{\partial y^*} = \mu \frac{\partial^2 u^*}{\partial y^{*2}} - \frac{\mu}{k^*} u^* - \frac{\sin^2 \xi}{1+m^2} \sigma B_0^2 u^* + \rho g \cos\alpha \, \beta_T (T^* - T_\infty) + \rho g \cos\alpha \, \beta_C (C^* - C_\infty) \tag{2}$$

$$\rho C_p v^* \frac{\partial T^*}{\partial y^*} = \alpha_1 \frac{\partial^2 T^*}{\partial y^{*2}} + \mu \left(\frac{\partial u^*}{\partial y^*} \right)^2 - \frac{\partial q_r^*}{\partial y^*} + \frac{\sin^2 \xi}{1+m^2} \sigma B_0^2 u^{*2} - Q_0 (T^* - T_\infty) \tag{3}$$

$$v^* \frac{\partial C^*}{\partial y^*} = D \frac{\partial^2 C^*}{\partial y^{*2}} - R(C^* - C_\infty) \tag{4}$$

$$\frac{\partial q_r^*}{\partial y^*} = 4I(T^* - T_\infty)' \tag{5}$$

Where $I' = \int_0^\infty K_{\lambda w} \frac{\partial e_{b\lambda}}{\partial T^*} d\lambda$, $K_{\lambda w}$ is one among the coefficient of absorption at the wall and $e_{b\lambda}$ is the Plank's function.

The relevant boundary conditions for velocity, temperature, and concentration fields are defined as follows under these assumptions

$$u^* = 0, \quad T^* = T_\infty, \quad C^* = C_\infty \qquad at \quad y = 0 \tag{6}$$

$$u^* \to 0, \quad T^* \to T_\infty, \quad C^* \to C_\infty \qquad as \quad y \to \infty \tag{7}$$

Initiating the non-dimensional parameters

$$u = \frac{u^*}{v_0}, \upsilon = \frac{\mu}{\rho}, R_1 = \frac{\upsilon (C_w - C_\infty) R_A}{v_0^2 \rho C_p (T_w - T_\infty)}, y = \frac{v_0 y^*}{\upsilon}, u_p = \frac{u_p^*}{v_0}, M^2 = \frac{B_0^2 \upsilon^2 \sigma}{v_0^2 \mu}, K = \frac{K^* v_0^2}{\upsilon^2},$$

$$\theta = \frac{T^* - T_\infty}{T_w - T_\infty}, C = \frac{C^* - C_\infty}{C_w - C_\infty}, Sc = \frac{\upsilon}{d}, \gamma = \frac{R\upsilon}{v_0^2}, \Pr = \frac{\mu Cp}{\alpha_1}, H = \frac{Q_0}{\rho C_p v_0^3}, F = \frac{4\upsilon I'}{\rho C_p v_0^2},$$

$$Ec = \frac{v_0^2}{C_p (T_w - T_\infty)}, Gr = \frac{\rho g \beta_T \upsilon^2 (T_w - T_\infty)}{v_0^3 \mu}, Gc = \frac{\rho g \beta_C \upsilon^2 (C_w - C_\infty)}{v_0^3 \mu} \tag{8}$$

where Gr, a modified Grashof number, is one of the parameters Hartmann number M, temperature dependent heat source parameter H, Hall current parameter m, porosity parameter K, inclination angle α, Schmidt number Sc, chemical reaction parameter, Grashof number Gm, Prandtl number Pr, Schmidt number Sc, the aligned angle ξ and the radiation parameter F,

The basic field equations (2) – (4), can be rewritten in the non-dimensional form as follows

$$\frac{\partial^2 u}{\partial y^2} + \frac{\partial u}{\partial y} - D_3 u = -D_1\theta - D_2 C \tag{9}$$

$$\frac{\partial^2 \theta}{\partial y^2} + \Pr\frac{\partial \theta}{\partial y} + \Pr Ec\left(\frac{\partial u}{\partial y}\right)^2 + \Pr EcM_1 u^2 - \Pr(F+\phi) = 0 \tag{10}$$

$$\frac{\partial^2 C}{\partial y^2} + Sc\frac{\partial C}{\partial y} - Sc\,\gamma\, C = 0 \tag{11}$$

Where $D_1 = Gr\cos\alpha$; $D_2 = Gm\cos\alpha$; $\mathrm{M}_1 = \dfrac{M^2\sin^2\xi}{(1+m^2)}$; $D_3 = \dfrac{1}{K} + M_1$;

The corresponding boundary conditions in non-dimensional form are:

$$u = 0, \theta = 1, C = 1 \qquad at \quad y = 0 \tag{12}$$

$$u \to 0, \quad \theta \to 0, \quad C \to 0 \qquad as \quad y \to \infty \tag{13}$$

3. RESULTS AND DISCUSSIONS

The current study examines the effects of chemical reaction (γ) and radiation absorption (R1) on transient free convection flow while taking into account mass and heat transfer in a magnetohydrodynamic (MHD) system. The radiative flow and free convective Joule heating are included in this system over a inclined porous moving surface. The study also takes into account heat sources that vary with temperature. Using perturbation techniques, the solutions for the velocity, temperature, and concentration fields are found with the following parameter values: Ec = 0.01, Gr = 4.0, Sc = 0.60, Pr = 0.70, K = 0.50, Gc = 2.0, α = π/6, F = 1.00, M = 2.00,ϕ = 0.10, ξ = π/4, γ = 0.10,. These parameter values apply to all graphs, unless explicitly stated otherwise on a specific graph. The study thoroughly examines the effects of various parameters on velocity, temperature, and concentration.

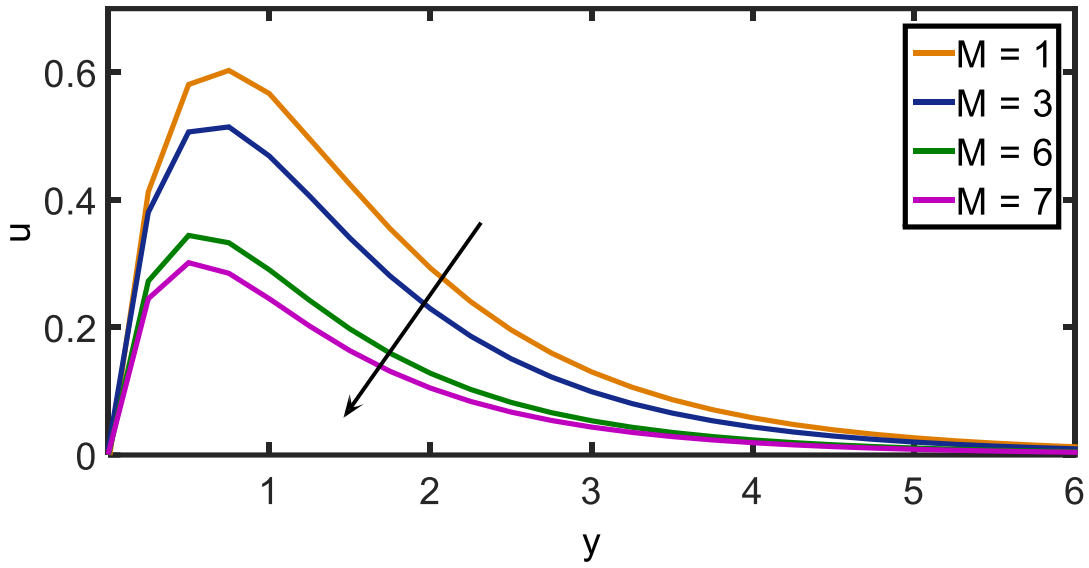

Figure 1: Velocity plots for dissimilar values of Hartmann number M.

These effects are meticulously analyzed through graphical representations. Moreover, the study delves into the behaviors of skin friction, rate of heat transfer and mass transfer rate with respect to different parameters. The results of these analyses are presented in tables for easy reference. The fluid velocity's behavior is specifically explored in Figures 1 to 6, illustrating its response to the influence of parameters M, K, α, Gr, Gc, and F. The Hartmann number (M)'s influence is depicted in Figure 1. It is clear that the velocity profiles gradually decrease as the values of M rise.

This phenomenon can be attributed to the interaction between transverse attractive fields and electrically-energized fluid flow. The Lorenz force generated in this context opposes the smooth flow of the liquid, resulting in increased flow resistance. Consequently, fluid velocity is retarded and boundary layer thickness increases. In Figure 2, the velocity plots for different values of the porosity parameter (K) are displayed. It's noticeable that as K increases, velocity also increasing. Figure 3 showcases the velocity profiles for different values of the magnetic field direction angle (α). Here, it's clear that velocity decreases with an increasing value of α. Moreover, the retardation force becomes more pronounced as the angle α increases. The impact of the Grashof number (Gr) on velocity profiles is demonstrated in Figure 4. As Grashof number increases, the velocity also increases. Figure 5 presents typical velocity profiles within the boundary layer for various values of the modified Grashof number (Gc). As anticipated, an increase in Gc leads to

higher fluid velocity, with a more distinctive peak value due to enhanced concentration buoyancy effects.

Figure 6 provides insight into the velocity profiles for different values of the radiation parameter (F). It's evident that higher F values correspond to lower peak velocity values, as increased radiation reduces the conduction effect of fluids. In Figure 7, velocity profiles for different Schmidt number (Sc) values are depicted. An increase in Sc leads to a decrease in velocity within the boundary layer. The influence of the Prandtl number on velocity profiles is shown in Figure 8. As the Prandtl number increases, velocity decreases. Figure 9 displays how the aligned angle (ξ) affects the velocity profile, revealing that an increase in ξ leads to a decrease in fluid velocity. Figure 10 illustrates velocity profiles for various Hall current parameter (m) values. Higher values of (m) result in decreased velocity distribution. Similarly, Figure 11 demonstrates the effect of the heat source parameter (ϕ) on velocity distribution, where increasing ϕ leads to decreased velocity. Turning to temperature effects, Figure 12 showcases the relationship between the radiation parameter (F) and temperature. With increasing F, temperature decreases due to reduced fluid conduction resulting from radiation. Figure 13 presents temperature plots for various values of Prandtl number, showing how higher Prandtl numbers lead to reduced temperature distribution.

Figure 14 analyzes the influence of the heat source parameter (ϕ) on temperature. As ϕ increases, temperature decreases. Figure 15 explores the concentration behavior for the various values of the chemical reaction γ, demonstrating that higher γ values lead to decreased concentration. Lastly, Figure 16 portrays the impact of the Schmidt number (Sc) on concentration, stating that as Sc increases, concentration found to be decreasing.

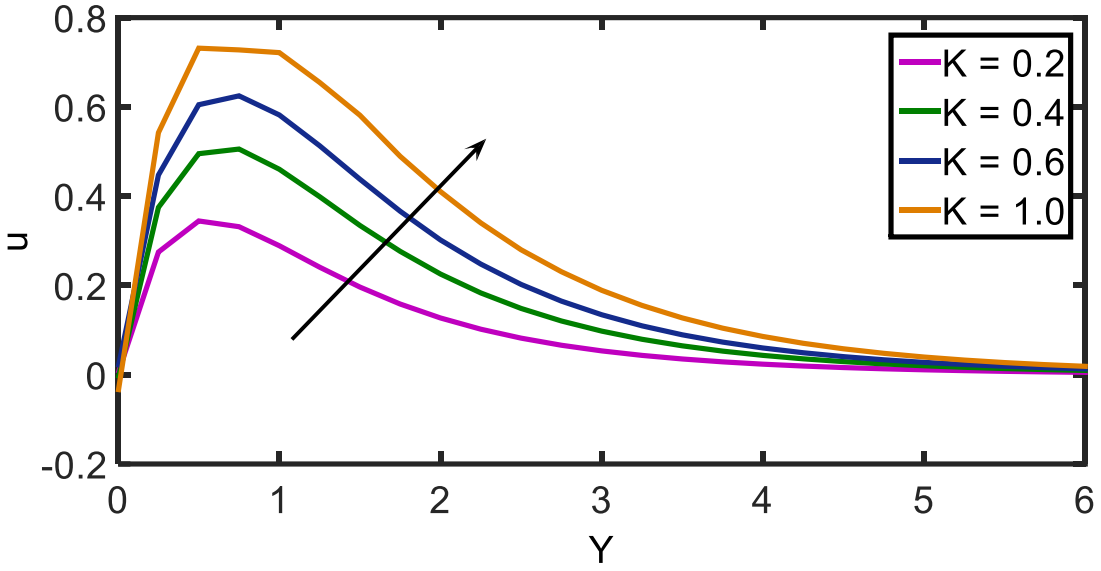

Figure 2: Velocity plots for dissimilar values of the porosity parameter K.

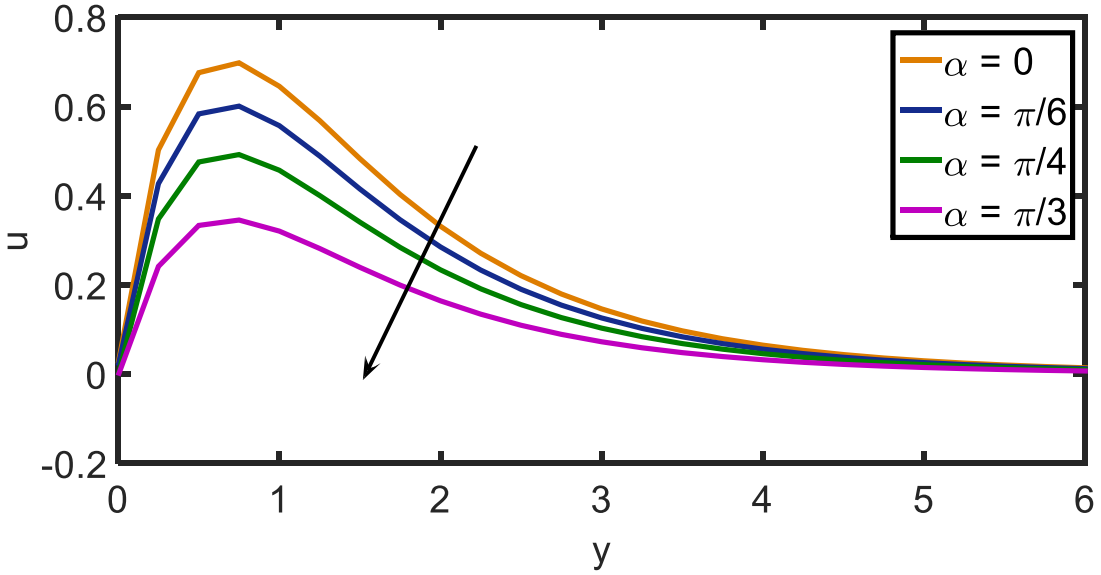

Figure 3: Velocity plots for dissimilar values of the angle of inclination α.

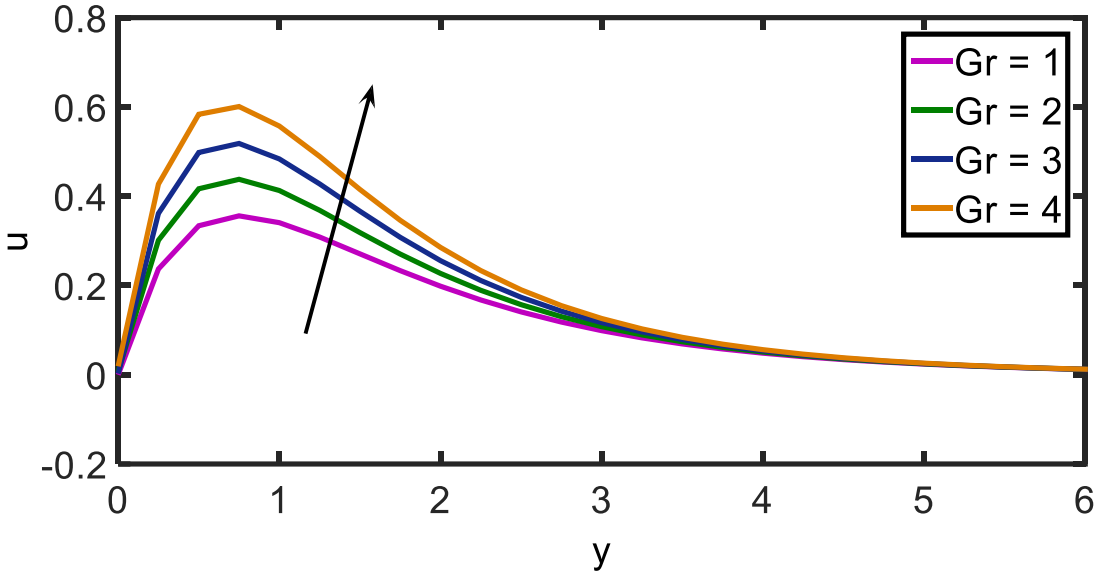

Figure 4: Velocity plots for dissimilar values of the Grashof number Gr.

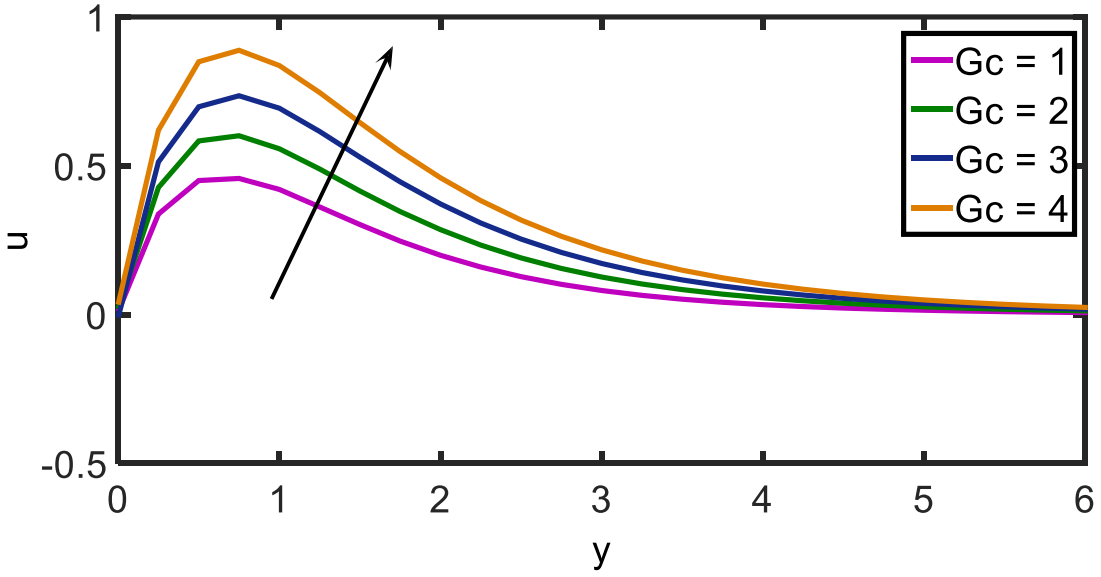

Figure 5: Velocity plots for dissimilar values of the modified Grashof number Gc

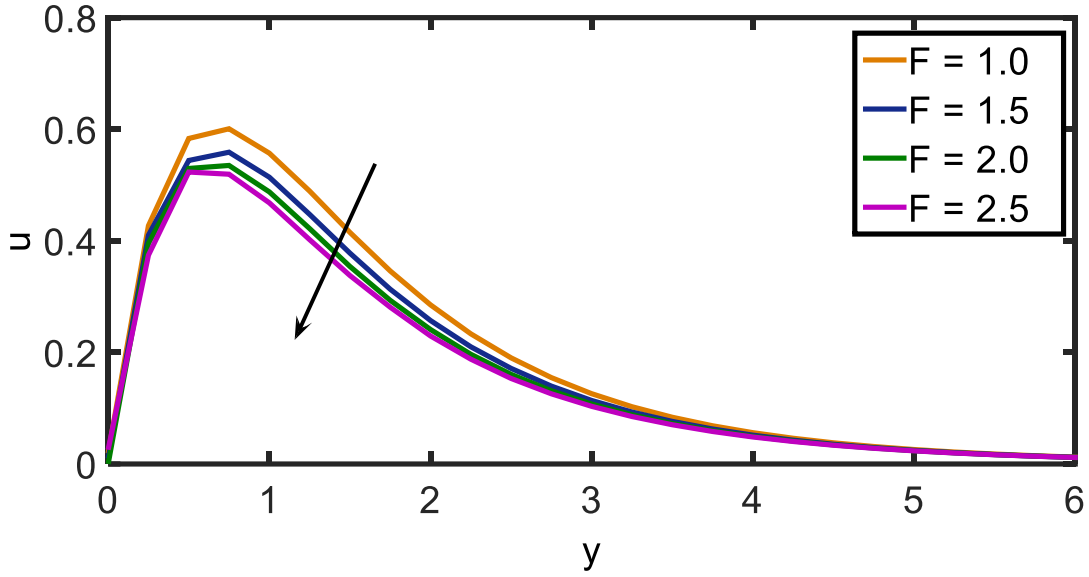

Figure 6: Velocity plots for dissimilar values of the radiation parameter F.

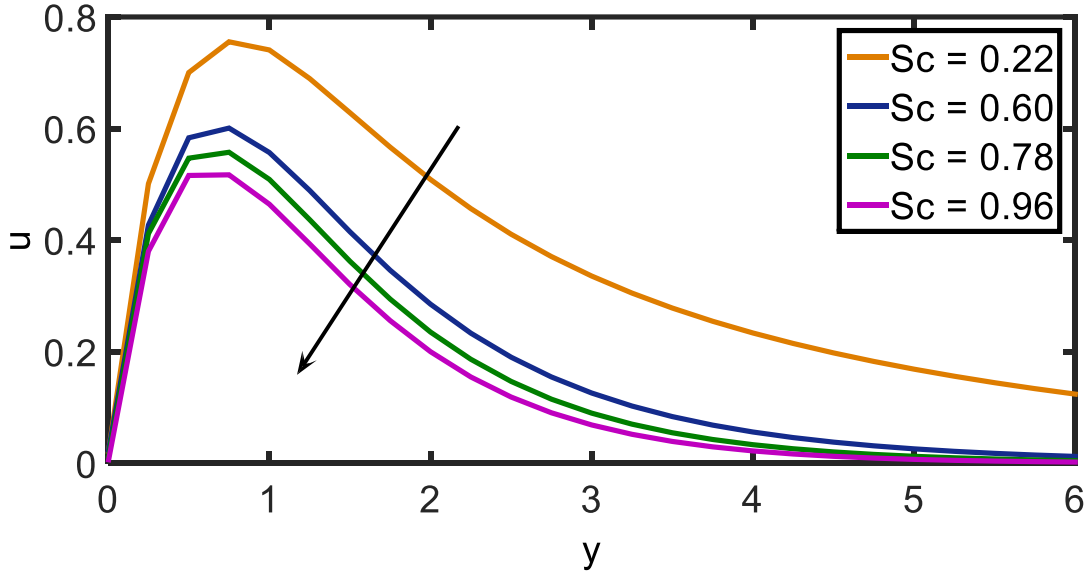

Figure 7: Velocity plots for dissimilar values of the Schmidt number Sc

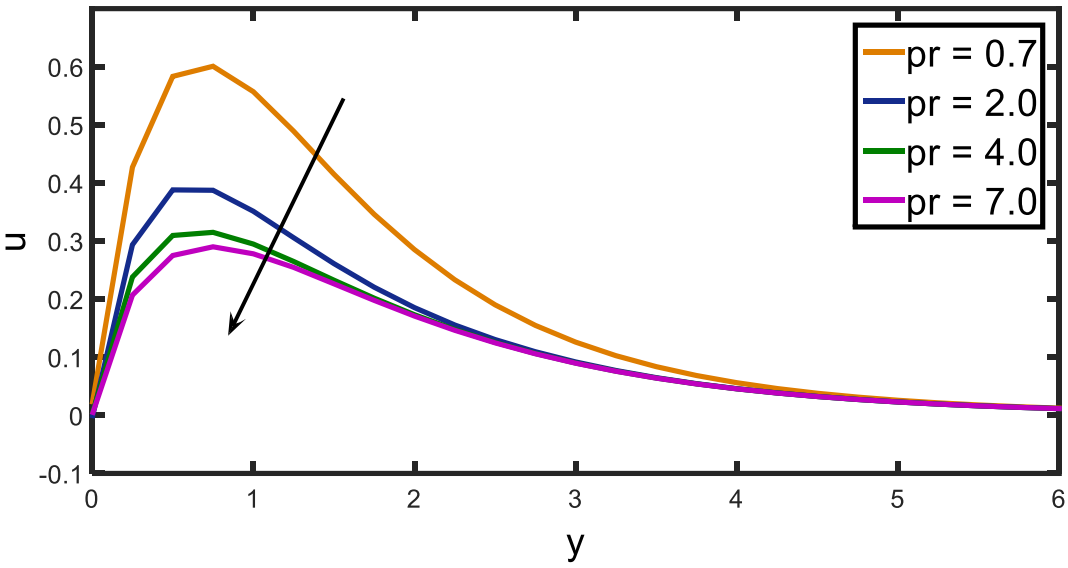

Figure 8: Velocity plots for dissimilar values of the Prandtl number Pr.

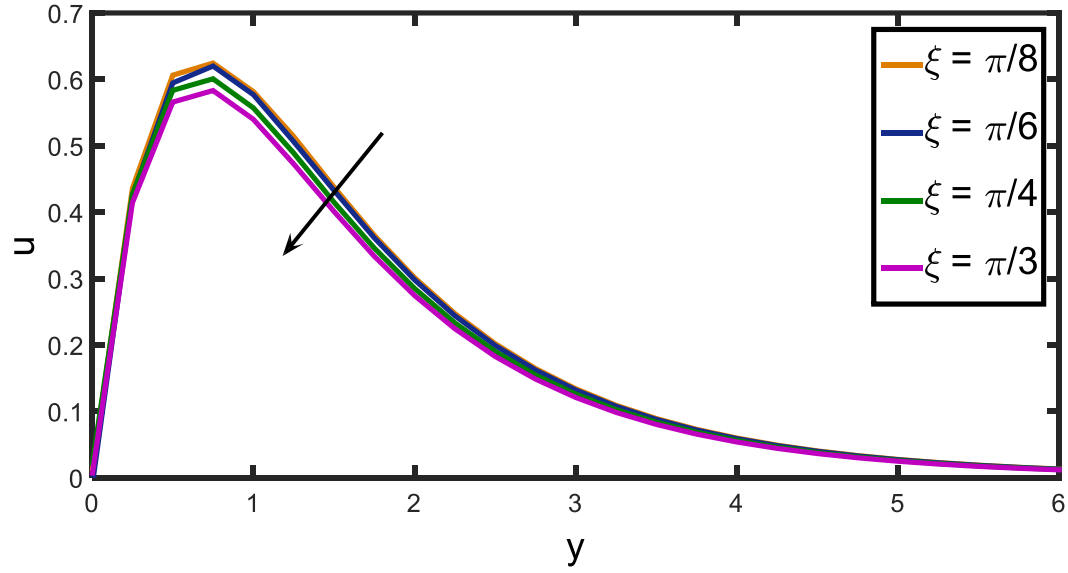

Figure 9: Velocity plots for dissimilar values of the aligned angle ξ.

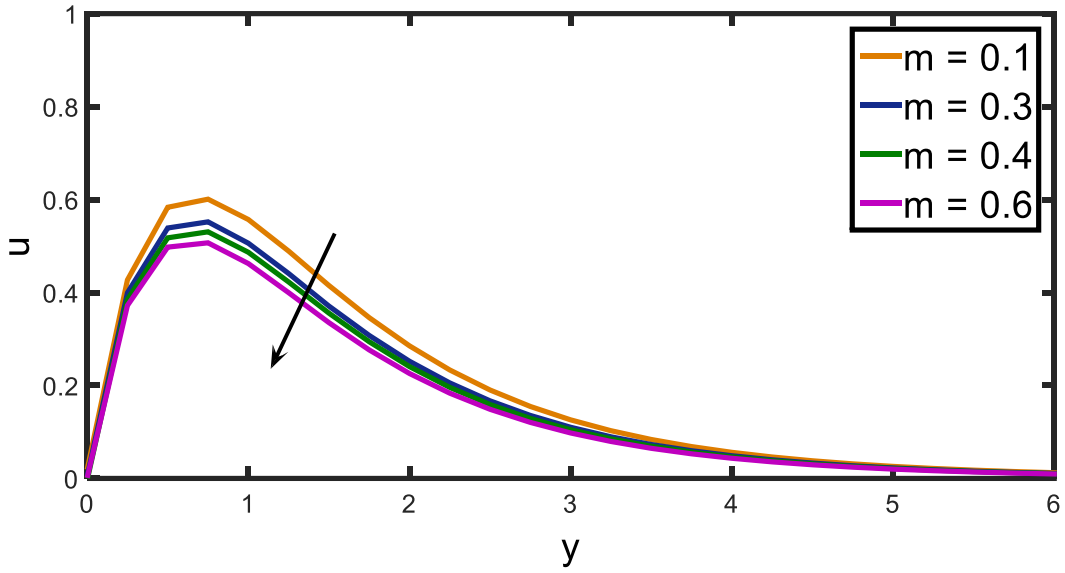

Figure 10: Velocity plots for dissimilar values of the Hall current parameter m.

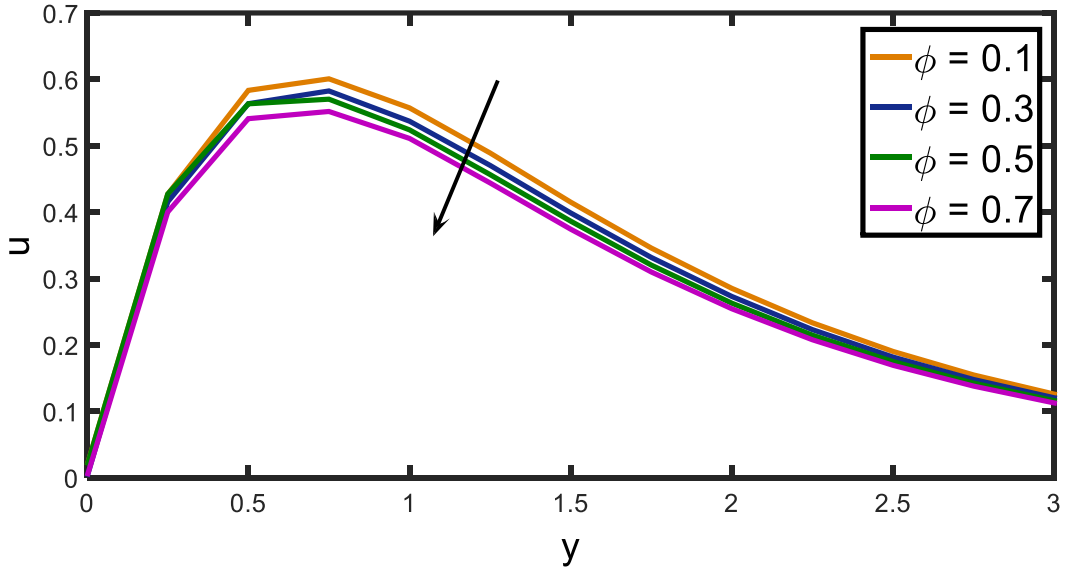

Figure 11: Velocity plots for dissimilar values of the heat source parameter ϕ.

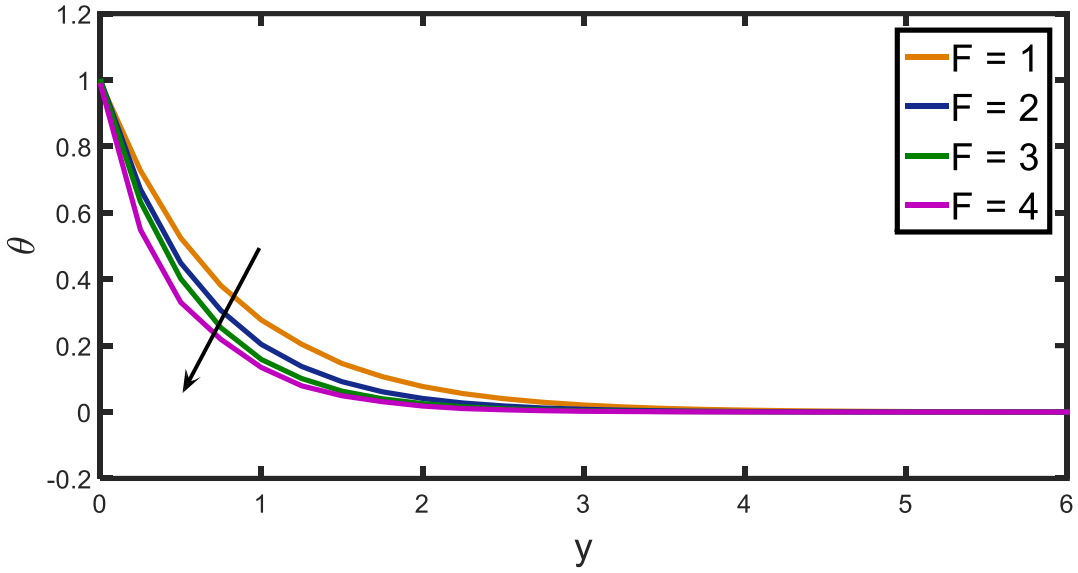

Figure 12: Temperature plots for dissimilar values of the radiation parameter F.

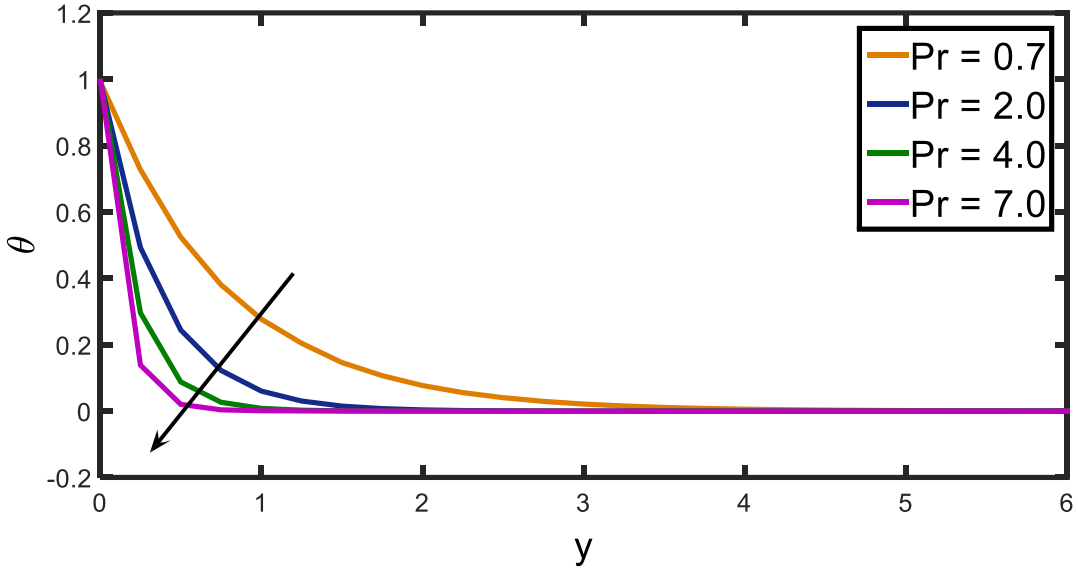

Figure 13: Temperature plots for dissimilar values of the Prandtl number Pr.

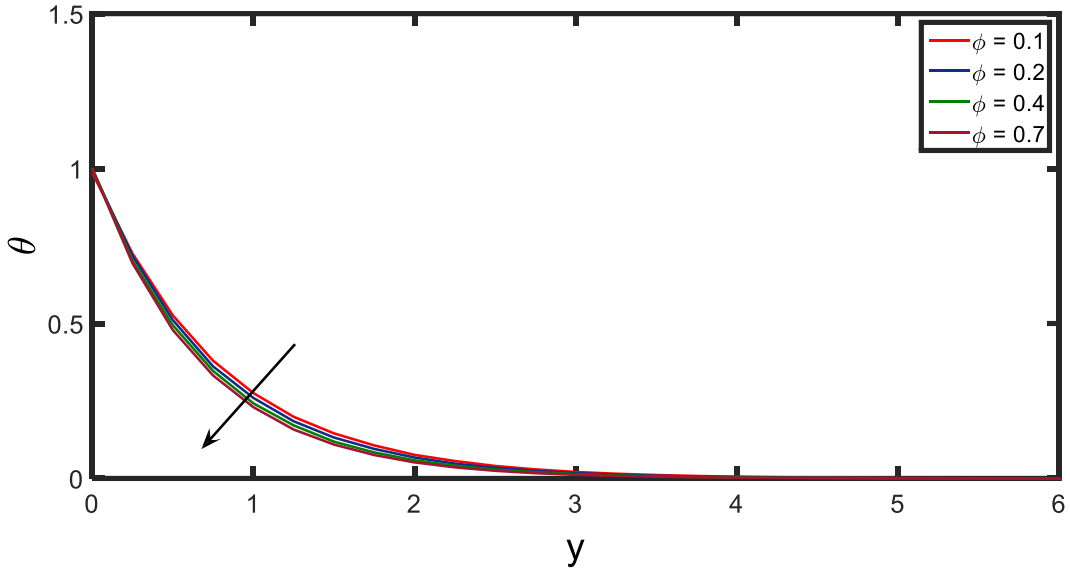

Figure 14: Temperature plots for various values of the heat source parameter ϕ.

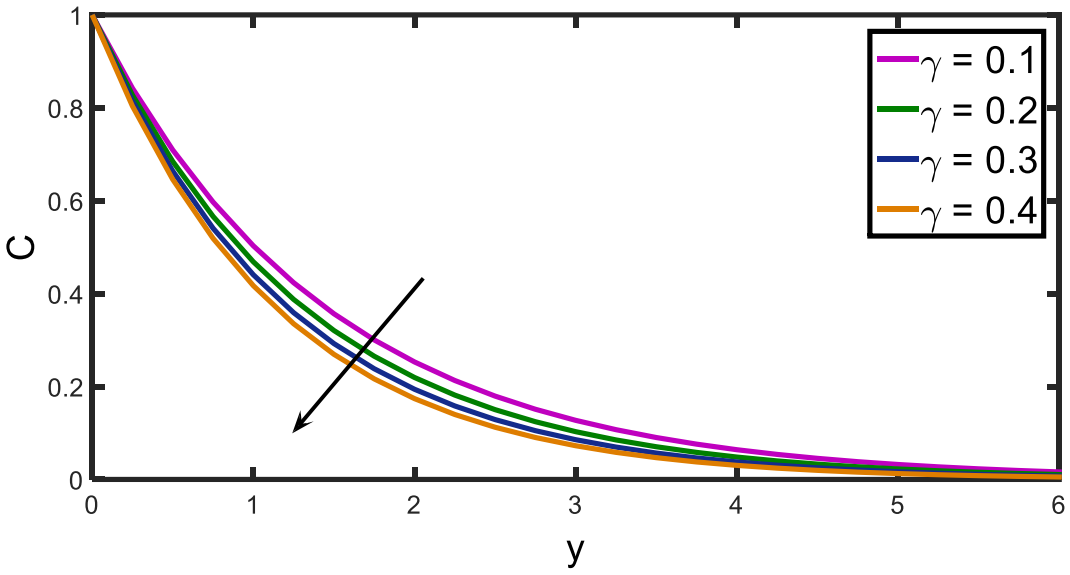

Figure 15: Concentration plots for dissimilar values of the chemical reaction parameter γ.

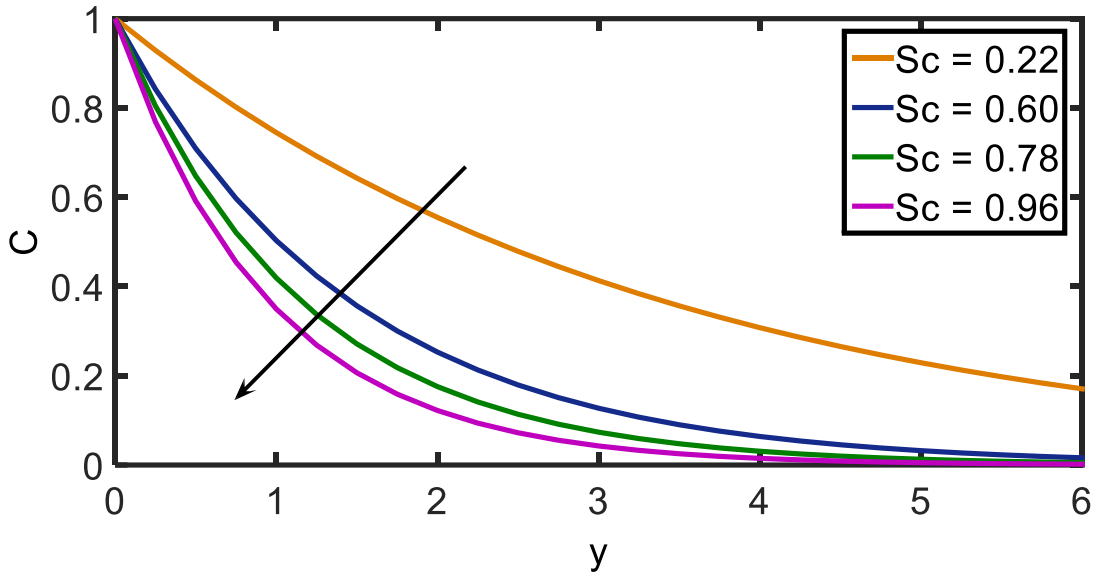

Figure 16: Concentration plots for dissimilar values of the Schmidt number Sc.

From the Table 1, we identified that the raising of Gr, Gc and K causes the skin-friction coefficient to increase. Also,it is observed that upon raising of F, M, ξ,, Sc, m and α the skin-friction decreases. From Table 2, it is observed that upon raising of Pr, F and ϕ the Nusselt number increases. From Table 3, we conclude that raising of Sc, γ causes the Sherwood number to decrease.

Table 1: The effects of various parameters on the skin-friction coefficient

M	**K**	**α**	**Gr**	**Gc**	**F**	**Sc**	**ξ**	**m**	**τ**
2.0	0.5	π/6	4.0	2.0	1.0	0.60	π/4	0.1	2.4355
4.0	0.5	π/6	4.0	2.0	1.0	0.60	π/4	0.1	2.2518
5.0	0.5	π/6	4.0	2.0	1.0	0.60	π/4	0.1	2.1895
2.0	**0.2**	π/6	4.0	2.0	1.0	0.60	π/4	0.2	1.7640
2.0	**0.4**	π/6	4.0	2.0	1.0	0.60	π/4	0.2	2.2138
2.0	**0.6**	π/6	4.0	2.0	1.0	0.60	π/4	0.2	2.5238
2.0	**0.9**	π/6	4.0	2.0	1.0	0.60	π/4	0.1	2.8048
2.0	0.5	**0**	4.0	2.0	1.0	0.60	π/4	0.1	2.8018
2.0	0.5	**π/4**	4.0	2.0	1.0	0.60	π/4	0.1	2.0406
2.0	0.5	**π/3**	4.0	2.0	1.0	0.60	π/4	0.1	1.4298
2.0	0.5	π/6	**1.0**	2.0	1.0	0.60	π/4	0.1	1.3586

2.0	0.5	π/6	**2.0**	2.0	1.0	0.60	π/4	0.1	1.7078
2.0	0.5	π/6	**3.0**	2.0	1.0	0.60	π/4	0.1	2.0941
2.0	0.5	π/6	4.0	**3.0**	1.0	0.60	π/4	0.1	3.0063
2.0	0.5	π/6	4.0	**4.0**	1.0	0.60	π/4	0.1	3.3969
2.0	0.5	π/6	4.0	**5.0**	1.0	0.60	π/4	0.1	3.9472
2.0	0.5	π/6	4.0	2.0	**1.2**	0.60	π/4	0.1	2.4395
2.0	0.5	π/6	4.0	2.0	**1.3**	0.60	π/4	0.1	2.4279
2.0	0.5	π/6	4.0	2.0	**1.4**	0.60	π/4	0.1	2.3582
2.0	0.5	π/6	4.0	2.0	1.0	**0.22**	π/4	0.1	2.7380
2.0	0.5	π/6	4.0	2.0	1.0	**0.78**	π/4	0.1	2.3690
2.0	0.5	π/6	4.0	2.0	1.0	**0.96**	π/4	0.1	2.3292
2.0	0.5	π/6	4.0	2.0	1.0	0.60	**π/12**	0.1	2.5663
2.0	0.5	π/6	4.0	2.0	1.0	0.60	**π/8**	0.1	2.4880
2.0	0.5	π/6	4.0	2.0	1.0	0.60	**π/3**	0.1	2.4271
2.0	0.5	π/6	4.0	2.0	1.0	0.60	π/4	**0.3**	2.3663
2.0	0.5	π/6	4.0	2.0	1.0	0.60	π/4	**0.4**	2.3113
2.0	0.5	π/6	4.0	2.0	1.0	0.60	π/4	**0.6**	2.2456

Table 2: The effects of various parameters on the Nusselt number

Pr	**ϕ**	**F**	**Nu**
0.7	0.1	**0.0**	0.8673
0.7	0.1	**1.0**	1.3776
0.7	0.1	**2.0**	1.7613
0.7	0.1	**3.0**	2.2887
0.72	0.1	1.0	1.4035
1.72	0.1	1.0	2.8416
2.72	0.1	1.0	3.5474
3.72	0.1	1.0	4.5931
0.7	**0.0**	1.0	1.3499
0.7	**0.1**	1.0	1.3776
0.7	**0.2**	1.0	1.4506
0.7	**0.3**	1.0	1.4578

Table 3: The effect of various parameters on the Sherwood number

γ	Sc	Sh
0.1	**0.22**	-0.2947
0.1	**0.60**	-0.6873
0.1	**0.78**	-0.8697
0.1	**0.96**	-1.0513
0.2	0.60	-0.7583
0.3	0.60	-0.8186
0.4	0.60	-0.8745

4. CONCLUSIONS

The influence of chemical reaction, Hall current, electrical conductivity, thermal radiation, and aligned magnetic field on the magnetohydrodynamic (MHD) fluid flow of a viscous, incompressible, and electrically-conducting fluid across a sliding porous inclined plate has been investigated theoretically. The governing equations are solved using a perturbation technique to obtain exact solutions. The key findings of this study can be summarized as follows:

- The concentration of the fluid diminishes as the Sc (Schmidt number) and γ (a parameter) increase.
- An increase in parameters ϕ, Pr (Prandtl number), and F results in a reduction in temperature.
- The velocity of the fluid flow enhances with higher values of Gr, Gc, α, F, and K, while it decreases with increasing values of M, Sc, Pr, ξ, m, and ϕ.
- The Sherwood number decreases as the Sc and γ increase.
- The Nusselt number rises with increasing values of Pr, F, and ϕ.
- The skin-friction coefficient increases with higher K, Gr, and Gc values, and decreases with elevated M, α, F, Sc, m, and ξ values.

REFERENCES

1. A. J. Chamkha, T. S. Reddy, M. C. Raju,and S. V. K. Varma, “unsteady MHD free convection flow past an exponentially accelerated vertical plate with mass transfer, chemical reaction and thermal radiation,” International Journal of Microscale and Nanoscale Thermal and Fluid Transport Phenomena, vol. 5, pp. 57-75,2014.

2. D. A. S. Rees and I. Pop, “Vertical free convection in a porous medium with variable permeability effects,” International Journal of heat mass transfer, 43, 2565-2571, 2010.

3. D. B. Ingham, I. Pop, and P. Cheng, “Combined free and forced convection in a porous medium between two vertical walls with viscous dissipation,” Transp Porous Media, vol. 5, no. 4, pp. 381–398, 1990.

4. J. C. Umavathi, A. J. Chamkha, and A. Mateen, “Unsteady Oscillatory Flow and Heat Transfer in a Horizontal Composite Porous Medium Channel,” Nonlinear Analysis: Modelling and Control, vol. 14, no. 3, pp. 397–415, 2009.

5. A. J. Chamkha, S. E. Ahmed, and A. S. Aloraier, “Melting and radiation effects on mixed convection from a vertical surface embedded in a non-Newtonian fluid saturated non-Darcy porous medium for aiding and opposing eternal flows,” International Journal of the Physical Sciences, vol. 5, no. July, pp. 1212–1224, 2010.

6. M.A.Hossain,“Viscous and Joule heating effects on MHD-free convection flow with variable plate Temperature”. International Journal of Heat and Mass Transfer, 35(12), 1992, 3485–3487.

7. M.A. Hossain, R.S. Gorla, “Joule heating effect on magnetohydrodynamic mixed convection boundary layer flow with variable electrical conductivity”, International Journal of Numerical Methods for Heat & Fluid Flow, Vol. 23(2), 275 – 288, 2013.

8. O.A. Bég, J. Zueco&H.S. Takhar, “Unsteady magnetohydrodynamic Hartmann–Couette flow and heat transfer in a Darcian channel with Hall current, ionslip, viscous and Joule heating effects: Network numerical solutions”, Communications in nonlinear science and numerical simulation, 14(4), 1082-1097, 2009.

9. C.H. Chen, “Combined heat and mass transfer in MHD free convection from a vertical surface with Ohmic heating and viscous dissipation”, International journal of engineering science, 42(7), 699-713, 2004.

10. N.A. Reddy, S.V.K. Varma, M. C. Raju, “Thermo diffusion and chemical effects with simultaneous thermal and mass diffusion in MHD mixed convection flow with Ohmic heating”, Journal of Naval Architecture and Marine Engineering, 6, 84-93, 2009.
11. P. Sibanda, O.D. Makinde, “On steady MHD flow and heat transfer past a rotating disk in a porous medium with Ohmic heating and viscous dissipation”, International Journal of Numerical Methods for Heat & Fluid Flow, 20 (3), 269 – 285, 2010.
12. A. Wang, C. Tu&X. Zhang, “Mixed convection of non-newtonian fluids from a vertical plate embedded in a porous medium”, ActaMechanicaSinica, 6 (3), 214-220, 1990.
13. K. A. Yih, “Viscous and Joule heating effects on non-Darcy MHD natural convection flow over a permeable sphere in porous media with internal heat generation”, International communications in heat and mass transfer, 27(4), 591-600, 2000.
14. R. Choudhury& S.K. Das, “Mixed Convective visco elastic MHD flow with Ohmic heating”, International Journal of computer applications, 68 (10), 7-13, 2013.
15. Raju M.C, C.Veeresh, S.V.K.Varma, Rushikumar B and Vijayakumar AG, “Heat And Mass Transfer In MHD Free Convection Flow on a Moving Inclined Porous Plate”, J Appl Computat Math ,4(5),1-7, 2015.